Annu. Rev. Biophys. Biomol. Struct. 1998. 27:329–56

CYTOCHROME *C* OXIDASE: Structure and Spectroscopy

H. Michel, J. Behr, A. Harrenga, and A. Kannt
Max-Planck-Institut für Biophysik, Frankfurt/Main, Germany;
e-mail: michel@mbibp-frankfurt.mpg.de

KEY WORDS: membrane protein crystallization, oxygen reduction, Raman spectroscopy, respiratory chain, X-ray crystallography

ABSTRACT

Cytochrome *c* oxidase, the terminal enzyme of the respiratory chains of mitochondria and aerobic bacteria, catalyzes electron transfer from cytochrome *c* to molecular oxygen, reducing the latter to water. Electron transfer is coupled to proton translocation across the membrane, resulting in a proton and charge gradient that is then employed by the F_0F_1-ATPase to synthesize ATP.

Over the last years, substantial progress has been made in our understanding of the structure and function of this enzyme. Spectroscopic techniques such as EPR, absorbance and resonance Raman spectroscopy, in combination with site-directed mutagenesis work, have been successfully applied to elucidate the nature of the cofactors and their ligands, to identify key residues involved in proton transfer, and to gain insight into the catalytic cycle and the structures of its intermediates. Recently, the crystal structures of a bacterial and a mitochondrial cytochrome *c* oxidase have been determined. In this review, we provide an overview of the crystal structures, summarize recent spectroscopic work, and combine structural and spectroscopic data in discussing mechanistic aspects of the enzyme. For the latter, we focus on the structure of the oxygen intermediates, proton-transfer pathways, and the much-debated issue of how electron transfer in the enzyme might be coupled to proton translocation.

CONTENTS

1056-8700/98/0610-0329$08.00

INTRODUCTION

Cytochrome *c* oxidases (E.C. 1.9.3.1) are the terminal enzymes in the respiratory chains from mitochondria and many bacteria. They use the electrons of cytochrome *c* to reduce molecular oxygen (dioxygen). The product of the reaction is water. It is essential that the complexes of the respiratory chains are integrated into the (inner) membranes of mitochondria or bacteria, because they create an electrochemical gradient of protons, consisting of a pH-gradient and an electric field, across the membrane. The electrochemical proton gradient drives protons back through the membrane via the ATP-synthases, which use this backflow of protons to synthesize adenosine-5′-triphosphate from adenosine-5′-diphosphate and inorganic phosphate. Adenosine-5′-triphosphate is the immediate energy source for numerous processes, including biosynthesis of many compounds, uptake of nutrients, and motility.

The protons needed for the formation of water originate from the inner side of bacteria or mitochondria, whereas cytochrome *c* resides on the opposite side of the membrane. This separation of the substrates leads already to the generation of an electrochemical proton gradient during the reaction cycle. In addition, cytochrome *c* oxidases have developed a mechanism to translocate ("pump") up to four protons across the membrane per reaction cycle, thereby doubling the yield of energy conversion.

Cytochrome *c* oxidases are members of the superfamily of heme/copper-containing terminal oxidases (6, 16, 23, 57, 84), which also comprises many ubiquinol oxidases, e.g. the well-studied cytochrome bo_3 from *Escherichia coli*, but not the cytochrome *bd* complex from the same bacterium (26). Membership of the heme/copper-containing terminal oxidase superfamily is indicated by the presence of histidine ligands to two heme groups and to a copper atom (Cu_B) in subunit I, which is the best-conserved subunit. In bacteria, the heme groups can be hemes A, B, or O (16), whereas only heme A is found in mitochondrial cytochrome *c* oxidases. A low-spin heme, heme *a* in the cytochrome *c* oxidases from mitochondria or the proteobacteria *Paracoccus denitrificans* and *Rhodobacter sphaeroides*, accepts electrons from ubiquinol or from a copper A (Cu_A) center bound to subunit II, and transfers them to a binuclear center. The

latter consists of a high-spin heme (heme a_3 in the cytochrome *c* oxidases from mitochondria and the proteobacteria), and a copper atom (Cu_B). Within the binuclear center, dioxygen is bound to the high-spin heme iron, reduced, and water is formed.

Subunit II is also well conserved. It is absent (or replaced) in some archaeal heme/copper-containing terminal oxidases, and, surprisingly, in an alternative oxidase complex of the nitrogen-fixing endosymbiont *Bradyrhizobium japonicum* (74). Subunit II contains the binuclear Cu_A center that receives the electrons from cytochrome *c* in cytochrome *c* oxidases. Consequently, the Cu_A center is absent in ubiquinol oxidases. Subunit III is also present in all mitochondrial and most bacterial heme-copper–containing terminal oxidases. In some bacterial and archaeal enzymes it (or a part of it) is fused to subunit I (17). As a result of their occurrence in most terminal heme-copper–containing terminal oxidases, subunits I-III are often called the core subunits. However, a complex consisting of subunits I and II of the cytochrome *c* oxidase from *P. denitrificans* is already fully active with respect to both dioxygen reduction to water and proton pumping (36).

As a consequence of their central position in metabolism, the cytochrome *c* oxidases have been intensively studied using biochemical, genetic, spectroscopic, and crystallographic tools. Nearly all conserved residues of subunit I have been mutated and the mutant enzymes have been characterized (43). The resulting structural predictions were found to be generally in good agreement with the structures obtained by X-ray crystallography. Time-resolved optical and resonance Raman spectroscopy (23, 49) has led to considerable insights into the catalytic cycle of this important enzyme. Successful crystallization was first reported in 1961 (117), but only recently crystals of a quality that allowed to determine the structure at high resolution have been obtained for the cytochrome *c* oxidases from *P. denitrificans* (45, 71, 72) and beef heart mitochondria (89, 90).

In this review, we summarize the results of the structure determinations as well as those of the various spectroscopic investigations. Special emphasis will lie on the coupling of oxygen reduction and proton movement in the light of the possible proton-transfer-pathways identified by mutagenesis work and X-ray crystallography.

HIGH-RESOLUTION STRUCTURES OF CYTOCHROME *C* OXIDASES

Overall Structure, Protein Subunits, and Prosthetic Groups

A landmark in the field of cytochrome *c* oxidase research was the determination of the three-dimensional structures of the bacterial cytochrome *c* oxidase from

the soil bacterium *P. denitrificans* (45, 72) and its mammalian counterpart from bovine heart mitochondria (89, 90). These structures now provide the scaffold for the interpretation of the results of spectroscopic studies and mutagenesis experiments, and for the functional discussion.

The key step in the structure determination of membrane proteins is to obtain suitable crystals for X-ray crystallography. This feat was achieved in the case of the bovine heart enzyme by extensive detergent screening and in the case of the bacterial enzyme by an approach of enlarging the polar surface with an F_v fragment of a monoclonal antibody combined with detergent screening (71, 72).

The cytochrome *c* oxidase from *P. denitrificans* consists of the three core subunits I, II, and III and a small non-conserved subunit IV of unknown function (109). The first crystals of the bacterial enzyme were obtained using the four-subunit cytochrome *c* oxidase (71). Later, an improved crystal form of the functionally active two-subunit cytochrome *c* oxidase complexed with the same antibody fragment as the four-subunit cytochrome *c* oxidase was observed, and the structure was determined at 2.7 Å resolution (72). The cytochrome *c* oxidase from beef heart mitochondria possesses ten small subunits in addition to the core subunits. It was crystallized in a dimeric form.

The structures of the bacterial and the mitochondrial enzymes are surprisingly similar. The core parts (subunits I, II, and III) of the two crystal structures look nearly identical at the atomic level. Figure 1 (*top*) presents the overall structure of the bacterial cytochrome *c* oxidase in a view perpendicular to the membrane normal. In this view, the cytochrome *c* oxidase looks like a trapezoid, with an extension at the smaller side. The trapezoid is integrated into the membrane. The extension represents the water soluble globular domain of subunit II. Figure 1 (*bottom*) shows a truncated form of the bacterial cytochrome *c* oxidase in a view from the periplasmic side along the membrane normal. In this projection, cytochrome *c* oxidase has an oval shape.

SUBUNIT III Although this subunit is present in nearly all cytochrome *c* oxidases, its function remains enigmatic. It does not contribute to the binding of

Figure 1 *Top*: Ribbon representation of the cytochrome *c* oxidase from the soil bacterium *Paracoccus denitrificans* in a view parallel to the membrane. *Light gray*, subunit I; *medium gray*, subunit II; *dark gray*, subunit III; *black*, subunit IV. The two copper atoms of the Cu_A-center can be seen at the top as *two black spheres*, heme *a* as atomic model in *black*, heme a_3 in *dark gray*. The Cu_B-atom is represented by a *black sphere* near heme a_3.

Bottom: View of the membrane part of the cytochrome *c* oxidase from *P. denitrificans* from the periplasmic side. Only the transmembrane helices, the heme groups (*dark gray*) and Cu_B (*black sphere* near heme *a*) are shown. The transmembrane helices are numbered and the location of pores A, B, and C is indicated. Prepared using MOLSCRIPT (51) and RASTER 3D (58).

(A)

(B)

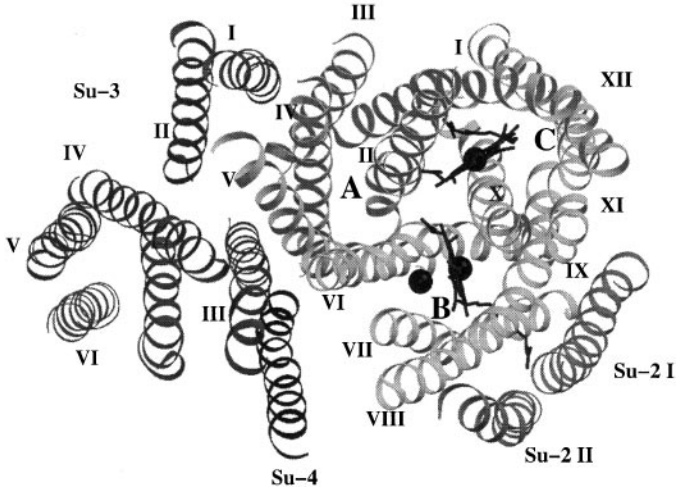
I
III
I
XII
Su–3
IV
II
II
C
IV
V
A
X
XI
V
IX
VI
B
III
VII
Su–2 I
VI
VIII
Su–2 II
Su–4

the cofactors nor is it necessary for proton pumping (36). Subunit III may be involved in the assembly of the cytochrome *c* oxidase (30) or form the entrance to a proposed oxygen channel leading to the active site (82; see below). It possesses seven transmembrane helices that are divided by a large V-shaped cleft into two bundles, one formed by the first two helices, and the other by helices III to VII. In this cleft, lipid molecules are firmly bound to conserved residues. A (putative) phosphatidylcholine has been incorporated into the atomic model of subunit III in the bacterial, and two phosphatidylethanolamine molecules and one phosphatidylglycerol molecule into that of the mitochondrial cytochrome *c* oxidase.

Subunit II Subunit II consists of two transmembrane helices interacting with subunit I and a large C-terminal extramembranous domain containing the Cu_A-center, which is located above subunit I in the periplasmic or intermembrane space (Figure 1). The structure of the extramembranous domain was also determined using a soluble quinol oxidase fragment containing an engineered copper center (107).

The fold of the globular domain containing a ten-stranded β-barrel is very similar to that of class I copper proteins like plastocyanin and azurin (2). The main difference is the presence of a mixed-valence [Cu(1.5)-Cu(1.5)] binuclear copper complex, which agrees with previous suggestions based on EPR data (10, 48), and the presence of only eight strands in the β-barrel of type I copper proteins.

The binding site for the two copper atoms, which can be seen in Figure 2, is formed by residues from strand 6 and the loop connecting strands 9 and 10. The ligands for each Cu atom form a distorted tetrahedron. Both copper atoms are ligated by two Cys residues and one His residue (Cu_A1: Su II-Cys 216,[1] Su II-Cys 220, Su II-His 181; Cu_A2: Su II-Cys 216, Su II-Cys 220, Su II-His 224).

Each Cu atom has an additional ligand: in one case a methionine (Cu_A1: Su II-Met 227) and in the other the carbonyl oxygen of a glutamate residue (Cu_A2: Su II-Glu 218). The two Cu atoms are bridged by the two cysteine thiolates, and the copper atoms and Cys sulfurs lie in one plane.

SUBUNIT I Subunit I is the largest and best conserved subunit of cytochrome *c* oxidase. It contains 12 transmembrane helices in an approximate threefold rotational symmetric arrangement. When viewed from the periplasmic side, the 12 transmembrane helices that are arranged in an anticlockwise sequential manner appear to form three symmetry-related semicircular arcs consisting of

[1]The sequence numbers refer to those of the subunits from the *Paracoccus denitrificans* cytochrome *c* oxidase. Table 1 contains the numbers of the homologous residues in the beef heart enzyme.

Table 1 Sequence number conversion table for important amino acid residues in subunits I and II of the cytochrome *c* oxidase from *P. denitrificans* and beef heart mitochondria

				Residue number	
				P. denitrificans	Bovine heart
Cu_A ligands		Su II	Cys	220	200
	Cu_A1	Su II	Cys	216	196
		Su II	His	181	161
		Su II	Met	227	207
		Su II	Cys	220	200
	Cu_A2	Su II	Cys	216	196
		Su II	His	224	204
		Su II	Glu	218	198
Heme ligands	*a*	Su I	His	94	61
		Su I	His	413	378
	a_3	Su I	His	411	376
Cu_B ligands		Su I	His	276	240
		Su I	His	325	290
		Su I	His	326	291
Mg ligands		Su II	Glu	218	198
		Su I	His	403	368
		Su I	Asp	404	369
Proton pathways		Su I	Lys	354	319
	K-pathway	Su I	Thr	351	316
		Su I	Tyr	280	244
		Su I	Asp	124	91
		Su I	Asn	199	163
		Su I	Asn	113	80
		Su I	Asn	131	98
	D-pathway	Su I	Tyr	35	19
		Su I	Ser	134	101
		Su I	Ser	193	157
		Su I	Glu	278	242
Electron transfer	$Cu_A \rightarrow$ heme a	Su II	His	224	204
		Su I	Arg	473	438
		Su I	Arg	474	439
	heme $\rightarrow$ heme a_3	Su I	Phe	412	377

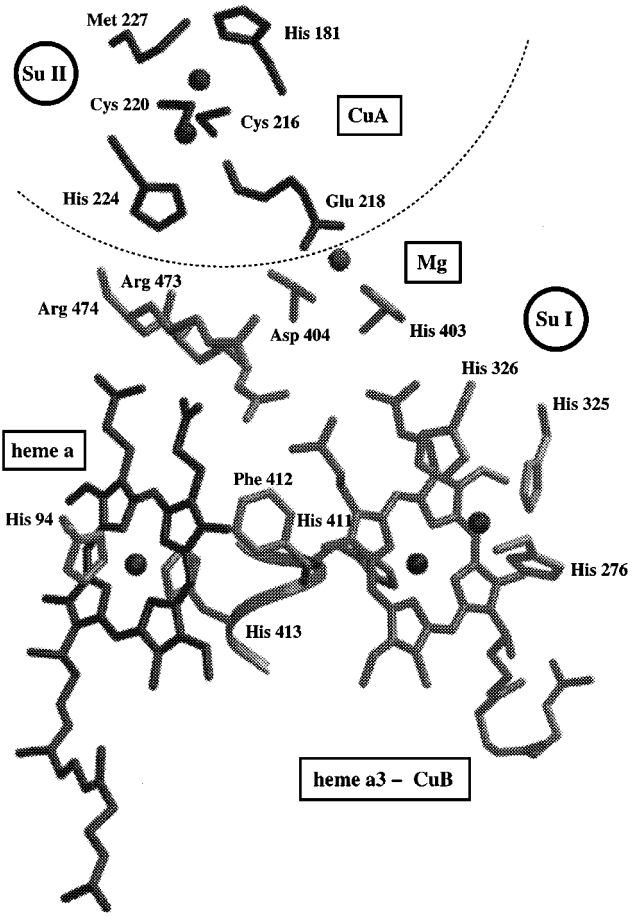

Figure 2 Atomic model for the prosthetic groups and neighboring amino acid residues in the cytochrome *c* oxidase from *P. denitrificans*. *Dark gray*, residues belonging to subunit II; *medium gray*, residues belonging to subunit I. *Spheres*, metals; *black*, heme *a*; *gray*, heme a_3. Prepared using MOLSCRIPT (51) and RASTER 3D (58).

four helices each (see Figure 1*B*, *bottom*). This arrangement generates three pores (A, B, C). Pore A is blocked by mostly conserved aromatic residues.

Subunit I contains the two heme groups, heme *a* being localized in pore C and heme a_3 in pore B. Heme a_3, together with a copper atom (Cu_B), forms the binuclear center that is the catalytic site for O_2 reduction. Both hemes are buried in the enzyme about 15 Å from the periplasmic surface. The heme planes are perpendicular to the membrane surface and the two propionate groups of each

point toward the periplasmic side. The heme groups approach each other to a distance of 4.5 Å and form an interplanar angle of 104° in the *P. denitrificans* structure.

Heme *a* is a low-spin heme with two conserved histidine imidazoles of helices II and X as axial Fe-ligands (Su I-His 94, Su I-His 413). In contrast to heme a_3, its hydroxyethylfarnesyl side chain points downward and remains in pore C. Together with the surrounding hydrophobic residues, it blocks access to heme *a* from the cytoplasm.

Heme a_3 is a high-spin heme. In the electron density, the iron appears to be fivefold coordinated. A conserved histidine imidazole of helix X is the axial Fe-ligand (Su I-His 411), which is two residues downstream from the heme *a* histidine ligand. The hydroxyethylfarnesyl group of heme a_3 leaves pore B and penetrates into the lipid bilayer, so that access of protons to the binulear center is principally possible from the cytoplasmic side of the membrane. The Cu_B ion is 4.5 Å away from the heme a_3 iron. It has three histidine imidazole ligands (Su I-His 276, Su I-His 325, and Su I-His 326). On the basis of strong antiferromagnetic coupling between Cu_B and heme a_3, a bridging ligand was proposed (73), but such a ligand is not clearly visible in the $[2F_o\text{-}F_c]$ electron density maps of the X-ray structures, and bridging by an amino acid side chain can be excluded. However, an $[F_o\text{-}F_c]$ difference map shows positive electron density between both metals. A combination of EXAFS and ENDOR spectroscopy suggests a fourth Cu_B ligand, most likely a water or a hydroxide ion, in the oxidized enzyme (22). A possible bridging structure is a hydroxide ion bound to Cu_B and hydrogen-bonded to a water ligand of the heme a_3 iron.

The cytochrome *c* oxidases—at least from mitochondria, *Rhodobacter sphaeroides*, and *P. denitrificans*—contain a non-redox–active Mn/Mg-binding site. In mitochondrial enzymes this site is occupied by Mg. Bacteria incorporate a substantial amount of manganese into this site when grown under Mg-limited conditions. This Mn/Mg-binding site is located at the interface between subunits I and II (see Figure 2). The Mg-ion is ligated by Su I-His 403, Su I-Asp 404, Su II-Glu 218, and at least one water (72, 90). An interesting feature is the arrangement of the carbonyl oxygen from Su II-Glu 218 also being a Cu_A ligand and of Su I-His 403 being hydrogen bonded to one of the heme a_3 propionates. Therefore, the Mg site lies directly between Cu_A and heme a_3. The function of the bound metal is not known.

ADDITIONAL SUBUNITS The bacterial cytochrome *c* oxidases have none or only one additional subunit (SU IV). The X-ray structure analysis of the *Paracoccus* enzyme revealed that the fourth subunit consists mainly of one transmembrane helix interacting with subunits I and III (45). Its function is unknown.

Even deletion of its gene has no obvious effect on the enzymatic properties, expression, and bacterial growth (109).

The mammalian cytochrome *c* oxidase from bovine heart has ten additional subunits. Again their function is unknown. The subunits Va and Vb are small globular proteins bound to the matrix side of the core, and the globular subunit VIb faces the intermembrane space. Subunit VIb binds a zinc ion of unknown function in a tetrahedral coordination. The subunits IV, VIa, VIc, VIIa, VIIb, VIIc, and VIII each possess one transmembrane helix. Subunit VIa seems to be responsible for the dimerization of the mitochondrial cytochrome *c* oxidase (90). It has been suggested that the small subunits act as regulators and bind effectors of enzyme activity like nucleotides (46) or are required for assembly. Tsukihara et al (90) propose two cholate binding sites as potential nucleotide binding sites. The presence of tissue-specific isoforms of several additional subunits supports the proposal of a regulatory function (52, 116).

Electron-Transfer Pathways

The crystal structures provide the distances between the metal centers and their relative orientations, the ligands, and the residues between them. Therefore, it is possible to obtain a deeper insight into the electron-transfer pathways.

Cu_A is generally accepted as being the primary electron acceptor from cytochrome *c* (37). The electron transfer rate between cytochrome *c* and Cu_A is very fast, about 70,000 s^{-1} (38). It has been proposed that the formation of the complex between cytochrome *c* and the cytochrome *c* oxidase is the rate-limiting step in the reaction between reduced cytochrome *c* and the oxidase (4). The nature of the binding is still unclear. The strong dependence on ionic strength is indicative for electrostatic interactions stabilizing the complex (4, 81). The corner formed by the globular domain of subunit II and the flat periplasmic surface of subunit I is most likely the cytochrome *c* binding site (45). This area contains ten exposed acidic residues that could interact with lysine residues at the heme edge of cytochrome *c*. Indeed, mutagenesis data have indicated a crucial role of these residues (110), although earlier work (53) using a soluble Cu_A domain of subunit II misidentified two residues as important that are actually deeply buried in the interface between subunits I and II.

From Cu_A the electron is transferred to heme *a* at a high speed (about 20,000 s^{-1}), considering the long metal-to-metal distance (19.5 Å) and small driving force (50 mV; 108). Iwata et al pointed out (45) that there is a conserved possible electron transfer pathway between Cu_A and heme *a* consisting of 14 covalent bonds and 2 hydrogen bonds. The Cu_A ligand Su II-His 224 forms a hydrogen bond to the carbonyl oxygen of Su I-Arg 473 located in the loop between the transmembrane helices IX and X. There are many contacts between residues in this loop and the heme *a* propionates. It seems that the combination

of a small reorganization energy for the Cu_A-heme *a* electron transfer caused by the binuclear structure of Cu_A (54) and the presence of an efficient electron transfer pathway is responsible for the rapid electron flow between the metal centers (79). Perturbation of the symmetrical nature of the binuclear Cu_A site indeed results in a strong inhibition of the enzyme (118). Direct electron transfer from Cu_A to heme a_3 is neglectably slow (1–100 s^{-1}), although it was suggested (37), and a regulatory function affecting the H^+/e^- stoichiometry was postulated (14). The crystal structure shows that the distances from Cu_A to the iron atoms of heme *a* and a_3 are 19.5 Å and 22.1 Å, respectively. This difference in distance, in combination with a much higher reorganization energy for Cu_A–heme a_3 electron transfer, could account for the large difference in transfer rates (13).

From heme *a* the electron is transferred to heme a_3. As mentioned, these hemes are nearly perpendicular to each other. While the iron-to-iron distance is 13.5 Å, the edges of the hemes approach each other up to 4.5 Å. An edge-to-edge electron transfer is therefore possible as well as a pathway using the iron ligands Su I-His 413 and Su I-His 411 and the polypeptide backbone. Another possibility mentioned (45, 90) is a pathway involving the side chain of the conserved Su I-Phe 412 that is placed approximately equidistant between the hemes (see also Figure 2).

Proton-Transfer Pathways

Based on the crystal structure of the *Paracoccus* enzyme and in agreement with the results of site-directed mutagenesis studies (24, 43, 88), two possible proton transfer pathways have been suggested (45), represented in Figure 3. The shorter one, also referred to as the K-pathway, leads to the binuclear center via the highly conserved residues Su I-Lys 354, Su I-Thr 351, and Su I-Tyr 280 located in the transmembrane helices VI and VIII, and the hydroxyl group of the heme a_3 hydroxyethylfarnesyl chain. The second, longer pathway (D-pathway) involves Su I-Asp 124 and a number of conserved polar residues (Su I-Asn 199, Su I-Asn 113, Su I-Asn 131, Su I-Tyr 35, Su I-Ser 134, and Su I-Ser 193) located around pore C (see Figure 1, *bottom*). Along the pathway, the proton would leave pore C toward Su I-Glu 278, most likely via a solvent-filled cavity. From there, the pathway is less clear but may involve Su I-Pro 277, from where it could reach the binuclear site. Alternatively, pumped protons could be transferred from Su I-Glu 278 to the heme a_3 propionates if these residues possess different conformations during the catalytic cycle.

Inspection of the bovine structure (90) revealed the same K-pathway, but the proposed D-pathway in the bovine structure does not lead to the binuclear site. It uses the same entrance, but after Su I-Ser 193 (*P. denitrificans* numbering; see Table 1 for conversion) it directly reaches the intermembrane space via polar

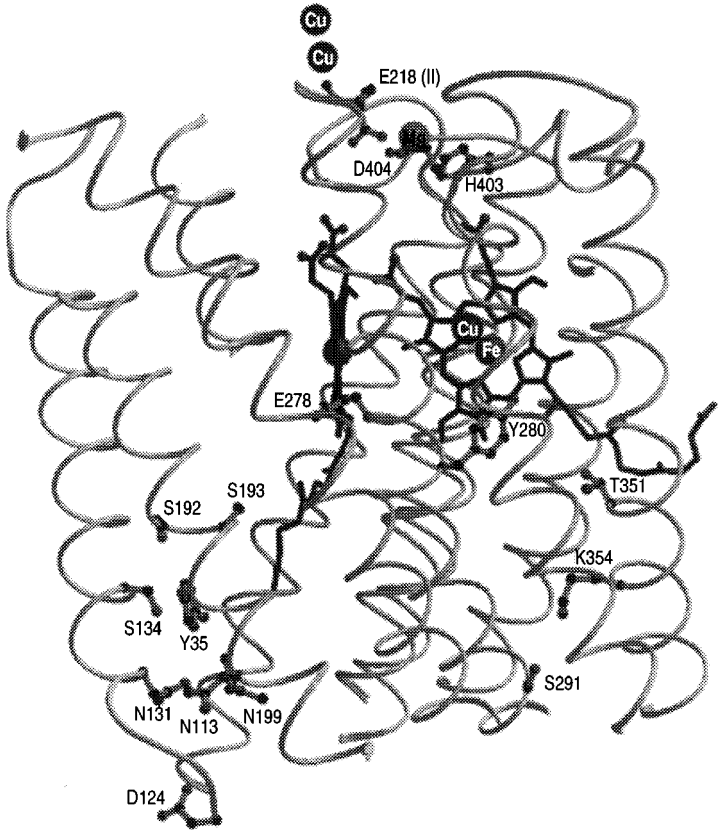

Figure 3 The transfer pathways for protons in the cytochrome *c* oxidase from *P. denitrificans*. The K-pathway including Su I-Lys-354 leads straight to the binuclear site. The D-pathway starting Su I-Asp-124 leads straight up to Su I-Ser-193 and then through a solvent-filled cavity to Su I-Glu-278. The further proton transfer pathway is unclear. It may lead to the binuclear heme a_3/Cu_B site, or to the propionate side chains of heme a_3. *Top*, Mg-binding site and Cu_A-center. Prepared using MOLSCRIPT (51) and RASTER 3D (58).

residues not conserved in the *P. denitrificans* enzyme. The latter residues are either alanines or glycines in the bacterial enzyme, thus leaving enough space for bound water allowing proton transfer (90). A third pathway passing heme *a*, which is located mainly between helices XI and XII of subunit I, was described (90). This pathway is also present in the *P. denitrificans* structure, with the exception of one residue. Mutagenesis data supporting these latter pathways do not exist.

Oxygen and Water Channels

For the beef heart cytochrome *c* oxidase, three hydrophobic channels were described and suggested as potential pathways for oxygen to reach the binuclear site (90). Some dynamic sidechain movements would still be needed to allow oxygen diffusion. The channels start at the protein-membrane interface near the center of the lipid bilayer, where oxygen solubility is much higher than in the aqueous phase. One of these channels has also been identified in the bacterial oxidase (82). It starts in the V-shaped cleft of subunit III directly above a tightly bound lipid molecule and leads through subunit I into the binuclear site. Whether oxygen channels are needed is not clear, because oxygen concentrations are high under physiological conditions.

A hydrophilic cleft between subunit I and II proceeds from the binuclear center to the outside of the membrane. This channel involves a number of charged residues and the Mg binding site. Tsukihara et al (90) suggested that this structure serves as an exit pathway for the water produced. Iwata et al (45), who favor a direct coupling of proton pumping, described this cleft as the exit pathway of the pumped protons from the binuclear center to the outside. Further experiments are needed to identify the correct interpretation.

OXYGEN REDUCTION AND ITS COUPLING TO PROTON MOVEMENT

Extensive biochemical and spectroscopic work has been performed to investigate the different oxygen species emerging during the reaction of cytochrome *c* oxidase with dioxygen and to determine the rates of the associated reaction steps.

The reaction of reduced or partially reduced cytochrome *c* oxidase with dioxygen is too fast to utilize conventional stopped-flow techniques. Therefore, a widely used method to initiate the reaction of the reduced enzyme with dioxygen is the flow-flash technique initially developed by Gibson & Greenwood (25, 27), where CO-bound reduced cytochrome *c* oxidase is photodissociated by a short laser flash after mixing with dioxygen-saturated buffer. A similar approach can be used to trap the incomplete forward reaction at intermediate points using the two-electron (18) or the three-electron reduced enzyme (111, 112). An important underlying assumption for the relevance of this technique is that the photodissociated CO does not interfere with the dioxygen reduction mechanism. The great advantage of this method is the high quantum yield in comparison to flash experiments with other ligands such as, for example, cyanide (41), so that a short laser flash results in a complete conversion of the CO complex to the oxy complex (6). However, the observation of the different oxygen

intermediates is very difficult, because the reaction with the fully reduced enzyme is extremely fast and the large optical absorbance changes caused by the redox events on the metal centers during the dioxygen reduction complicate the observation of the much smaller changes associated with the oxygen chemistry. Nevertheless, time-resolved optical absorption spectroscopy was used to investigate the kinetics of electron transfer (38, 40, 68, 70, 94) and to determine the spectral characteristics of intermediates (61). EPR studies (12, 35, 47, 111, 112) as well as low-temperature optical absorption measurements (18, 19) have also provided information about some transient intermediates during the reaction with dioxygen. A wealth of information about the structural features of some intermediates has been derived by Raman spectroscopy (32–34, 64–67, 75–77, 91–93).

Adopting a different approach, Wikström (103) originally showed the existence of the different oxygen intermediates in an experiment on intact mitochondria, where he managed to partially reverse the oxygen reaction by energizing mitochondria with ATP, resulting in a backward electron flow.

Two oxygen species have also been generated artificially by addition of different amounts of hydrogen peroxide to the oxidized enzyme (115). Detailed information about these reactions can be obtained from an article by Fabian & Palmer (21).

The Ferrous-Oxy Species

Figure 4 summarizes the catalytic cycle of cytochrome *c* oxidase with respect to the oxygen chemistry. Starting at the fully oxidized enzyme (O), the first intermediate formed is the one-electron reduced or E-state, where the electron equilibrates between heme *a* and the binuclear center (62). It has been suggested (95) that the rate of electron transfer from heme *a* to the binuclear center is proton-controlled in that protonation of a site close to the binuclear center is required to raise the redox potential of heme a_3, thus stabilizing its reduced form. Uptake of the second electron yields the two-electron reduced or R-state, where dioxygen can bind to the reduced heme a_3. The rate of this initial binding reaction, however, is not proportional to $[O_2]$ but saturates at high concentrations of oxygen (27, 56), thus suggesting transient ligation to another site prior to binding to the heme.

Additional evidence has been provided that the initial O_2 adduct does not involve heme a_3 (11). Thus, initiated and supported by the observation of transient but quantitative binding of CO to Cu_B after photolysis from heme a_3 (3, 20), the copper has been proposed as the first binding site for the incoming oxygen (114). Oliveberg & Malmström (69) have attributed absorbance changes at 830 nm to the formation of this Cu_B-O_2 adduct, and the second-order forward rate constant for the Cu_B-O_2 association has been determined

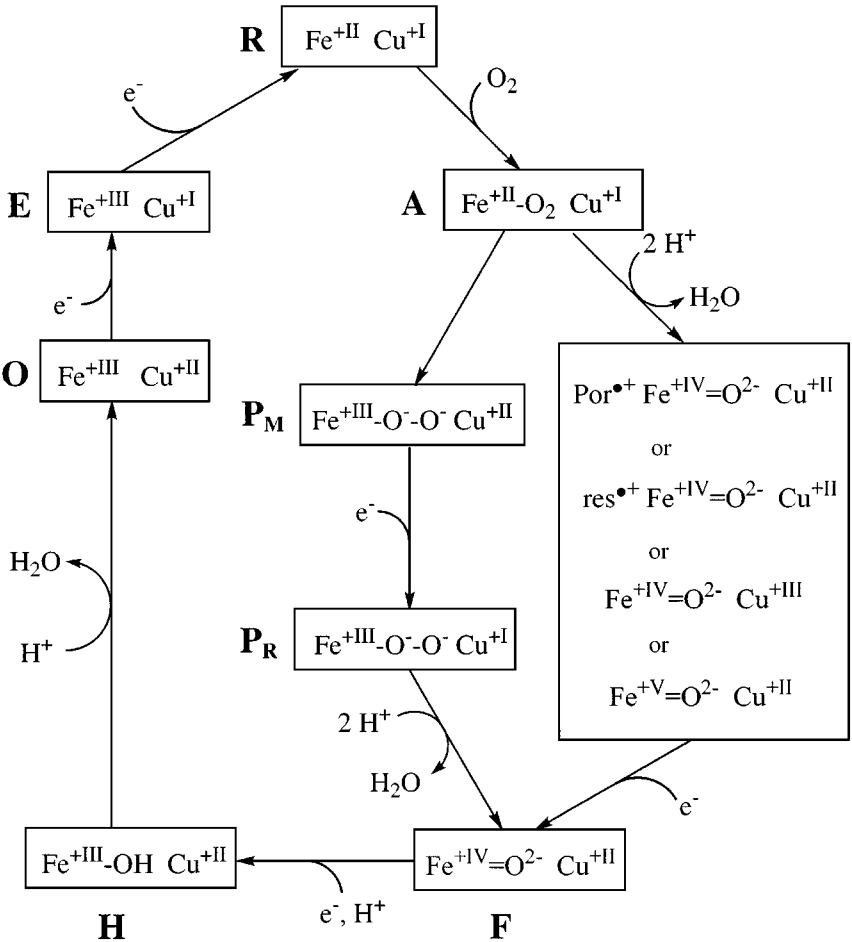

Figure 4 The catalytic cycle of cytochrome *c* oxidase as derived from optical and resonance Raman spectroscopy (23, 49). Starting from the oxidized form (*O*), the one-electron reduced form (*E*) and then the doubly reduced form (*R*) are generated. Upon oxygen binding compound A is observed. Next the peroxy-intermediates P_M, P_R are formed (see also text). Alternative structures are presented on the *right*, based on the proposal that the O-O bond is already split in these states. However, one electron is missing, which could be provided by a porphyin-ring system (por), an amino acid residue (res), Cu_B (leading to a Cu^{3+}-state), or the heme a_3-Fe. There is general agreement about the structure of the oxoferryl-state (*F*) and a hydroxy-state (*H*) formed after protonation of the iron-bound oxygen atom. After water formation and release, the O-state is regenerated.

as 3.5×10^8 M^{-1} s^{-1} (11). Because the binding is transient, the interaction between O_2 and Cu_B is only weak ($K_D = 8$ mM; 8, 94).

The ferrous-oxy species was first observed at low temperatures by Chance and co-workers (18) and termed compound A. At room temperature, it is characterized by an increase in absorbance (relative to the unliganded reduced enzyme) at 595 nm and 430 nm (39, 96) and the ν(Fe-O_2) stretching mode at 572 cm^{-1} (32, 64, 91) in the resonance Raman spectrum that shifts to 546 cm^{-1} when $^{18}O_2$ is used (91). This frequency is well reproduced by an imidazole-heme A-O_2 model compound (63) showing that, similar to oxyhemoglobin, O_2 forms a relaxed, low-energy complex with the ferrous heme and that there are only small distal pocket effects and little interaction of the oxygen with Cu_B (5). Oliveberg & Malmström (69) have determined the pseudo-first–order rate of O_2 binding to be 1×10^5 s^{-1}, in good agreement with values found by Verkhovsky et al (94) and Bailey et al (8). Again, the O_2 association is weak, with a K_D of ~0.3 mM (18, 40, 94).

Electron Transfer and Oxygen Intermediates in the Mixed-Valence Enzyme

The further decay of the oxygen species depends upon the redox state of the enzyme. In the case of the mixed-valence enzyme where no further electrons are available, compound A, through electronic reorganization within the binuclear center, is converted to the so-called compound C (18) at a rate of 5×10^3 s^{-1} (40, 68, 93). At room temperature, this species is characterized by a strong absorbance band at 607 nm ($\epsilon\{607–630\text{ nm}\} = 11$ $mM^{-1}cm^{-1}$; 106), and a red-shift of the Soret band to 428 nm. A similar species is observed in the reaction of the oxidized enzyme with low concentrations of hydrogen peroxide at alkaline pH (9, 21, 50, 102) and in reversed-electron flow experiments as the result of a two-electron reversal (103). However, the structure of this species, which is at a redox level two electrons above the oxidized enzyme, has remained a matter of debate. Previous proposals include a ferric-cupric peroxy species P_M (*M* stands for mixed valence) (Figure 4) (6, 61), a ferryl-cupric (Fe(IV)=O Cu(II)) species with an additional protein radical (101, 102), and a Fe(IV)=O Cu(III) form (21). The latter two are supported by Raman studies of the oxidized enzyme/peroxide reaction, where 607-nm excitation yielded a 803 cm^{-1} mode that was shifted to 769 cm^{-1} when the reaction was initiated with $H_2{}^{18}O_2$ (75) and thus assigned to a ferryl species. However, this Raman mode has not been observed in cytochrome bo_3 (42), though the oxygen intermediates are the same in the bo_3- and aa_3-type terminal oxidases (60). Additionally, the absorbance spectrum of the 607-nm species observed in the reaction of the fully-reduced enzyme (P_R) is nearly identical to that of P_M, although P_R is at a redox level one electron above P_M, thus favoring a peroxy-type structure for P_M (61; see below).

Oxygen Reduction in the Fully-Reduced Enzyme

The reaction of the fully-reduced enzyme with dioxygen differs from that of the mixed-valence form in that two more electrons are available that can be transferred to the binuclear center after oxygen binding. Again, compound A is formed first (Figure 3). However, compared to the mixed-valence/oxygen reaction, the subsequent electronic step is much faster, namely 3×10^4 s^{-1} (32, 37, 68, 93, 94) and has been attributed to electron transfer from the reduced heme *a* to the binuclear center (34, 37). Thus, the redox state of the binuclear center in the newly formed species is formally three reducing equivalents above that of the oxidized enzyme, and, assuming a peroxy-like structure, the species was termed P1 (94) or P_R (reduced; 61). It has been shown very elegantly by Verkhovsky et al (97) that it is the heme-heme electron transfer and thus the formation of P_R that traps the oxygen within the binuclear center. As already mentioned above, the spectral properties of P_R are nearly indistinguishable from those of P_M, suggesting that the redox state of heme a_3 and the configuration of the heme-oxygen moiety are the same in the two species (61, 86). As for P_M, the structure of P_R is yet unknown and has been debated extensively over the last years. Two Raman modes at 804 and 356 cm^{-1} have been associated with the two intermediates but interpreted differently by different research groups. Varotsis et al (93) assigned the latter mode to a $\nu(Fe^{3+}\text{-}O^-)$ stretching vibration, thus suggesting a ferric-cuprous peroxy species for P_R (Figure 4), while a ferrous-cupric peroxy form has been proposed by Blair et al (12), because they observed an EPR-active intermediate at low temperature, and by Babcock et al (7). However, Kitagawa and co-workers (49, 67, 75, 76) assign the 356 cm^{-1} mode to a $Fe^V{=}O$ bending motion, thus assuming that the O-O bond is already broken at this stage of the catalytic cycle (Figure 4) (23, 49). It has been pointed out by Morgan et al (61) that, in the light of identical absorbance spectra for P_M and P_R, the ferryl-type structures (21, 101, 102) proposed for P_M seem unlikely. If P_M had the $Fe^{IV}{=}O\ Cu^{III}$ structure proposed by Fabian & Palmer (21) then P_R, which is one electron more reduced, would most likely be $Fe^{IV}{=}O\ Cu^{II}$. The latter structure, however, has been unequivocally assigned to intermediate F (see below). Because P_R and F have been shown to be distinct intermediates in the catalytic cycle (61), the P_M structure suggested by Fabian & Palmer seems unlikely. The same is true for the oxoferryl structure with the protein radical, because such a radical species cannot account for the spectral differences between P_M and F as outlined by Morgan et al (61; see also below).

The Ferryl and Hydroxy Species

Proceeding from the P_R state, a ferryl-cupric species F is produced on a time scale of $t = 200\ \mu s$ without further electron input into the binuclear center. This intermediate exhibits a characteristic absorption maximum in the optical

difference spectrum (ferryl minus resting) at ~580 nm and it is well established that the 785 cm^{-1} mode observed in resonance Raman spectra and assigned as a $\nu(Fe^{IV}{=}O)$ stretching mode in $^{16}O_2/^{18}O_2$ mixed-isotope experiments is due to this ferryl species (34, 64, 92). Unexpectedly, this 785 cm^{-1} species was determined to shift to 795–800 cm^{-1} in D_2O experiments (33, 65, 93), which can hardly be explained if a simple $Fe^{IV}{=}O$ mode is assumed. Han et al (33) have concluded that the ferryl-oxo complex is hydrogen-bonded in H_2O but nonhydrogen-bonded in D_2O, which implicates large structural changes upon deuteration. Ogura et al (67) and Proshlyakov et al (76) assigned the 800 cm^{-1} mode in D_2O to an earlier intermediate in the cycle, which appears at a different time scale because of a significant slowing down of the reaction by the H_2O/D_2O exchange.

The ferryl intermediate can also be generated by a one-electron oxidation of the binuclear center in reversed O_2-reduction experiments (103, 106) or by carefully adding three electrons to the enzyme and further mixing with dioxygen (111, 112). The same state could be obtained by the flow-flash technique using quinol oxidases that contain three electrons in their fully reduced state because of the lack of the Cu_A center (55).

The conversion of the P_R to the F state is accompanied by electron transfer from Cu_A to heme *a*, resulting in an 50/50 equilibration between the two redox centers, so that the electron hole at heme *a* produced in the previous phase of the reaction is partially filled up (61, 86). This event was suggested to be initiated by the oxidation of Cu_B because of the anticooperative interaction between Cu_B and heme *a* (69). This implies that the oxidation of Cu_B is linked to a conversion of the low-potential heme *a* to a high-potential heme *a*, resulting in the electron transfer from the Cu_A to heme *a*. This process occurs on a similar or faster time scale as the formation of the ferryl intermediate ($\tau = 100$–$140\ \mu s$; 37, 38, 40, 68) and could be detected as a restoration of absorbance at 440 nm in the optical spectrum (21, 94). The partial oxidation of Cu_A was also shown directly by an increase in absorption at 830 nm at room temperature ($\tau = 170\ \mu s$; $k = 6 \times 10^3\ s^{-1}$; 40). Recently, Morgan et al (61) have provided evidence that the peroxy species decays into the 580-nm species F at the same time as the low-spin heme becomes partially re-reduced by Cu_A at $-25^\circ C$.

The rate of the P $\rightarrow$ F transition is pH-dependent, decreasing at increasing pH with a pK_a of 7.9, and as mentioned above, the reaction rate is lowered by H_2O/D_2O exchange. The value obtained for k_H/k_D was 1.4 for this phase (29). These observations led to the suggestion that the rate is limited by proton uptake, which is also supported by the fact that the rate of proton uptake monitored using pH indicators is similar to the rate of the redox reaction (29). Moreover, the pH dependence of the proton uptake parallels that of the redox

reaction and the observed deuterium isotopic effect of the proton uptake was also determined to be 1.4 (29). Oliveberg & Malmström (69) therefore proposed that the formation of the F species is controlled by protonation at the binuclear center.

The conversion of the P_M state discussed above to the ferryl state can be obtained by input of a single electron using a photoinducible reductant, which confirms that P_M differs fom F by one electron equivalent (98).

Finally, the F species is reduced by the fourth electron accompanied with the uptake of a proton (29), which leads to the formation of a new species detectable by Raman spectroscopy. The resulting ferric-hydroxy species (H) is characterized by a resonance Raman line at 450 cm^{-1} (31, 33, 65–67, 93) appearing with a rate constant of 800–1000 s^{-1} (29, 38, 68). This fourth phase has also been shown to be pH-dependent and to have a D_2O isotope effect. Like the third phase, this step is suggested to be rate-limited by proton uptake from the medium (29). The following uptake of another proton leads to the ferric/cupric O-state after the release of the second water molecule, so that the dioxygen reduction cycle is completed.

The Coupling of Electron Transfer and Proton Motion

As described above, oxygen reduction in terminal heme-copper oxidases is coupled to proton translocation from the cytoplasm or the mitochondrial matrix ("the i-side") into the periplasm or mitochondrial intermembrane space, thus generating a proton and charge gradient across the membrane. However, the mechanism by which the two processes are coupled to each other at the molecular level remains unclear. In principle, two different schemes are feasible: an indirect mechanism in which the redox chemistry is associated with major conformational changes in the protein, or a direct mechanism where the coupling is achieved by subtle changes occurring very close to the redox centers, e.g. through the involvement of metal ligands. The former has been suggested by Tsukihara et al (90) on the grounds of their proposed proton pathways separated from the oxygen chemistry in the crystal structure of the bovine-heart enzyme. However, many other groups have focussed on a direct coupling since the energy required for proton translocation must be supplied by the oxygen chemistry, and the binuclear centers of the heme-copper–containing terminal oxidase superfamily share a common structure (80).

"Scalar" protons required for water formation are generally distinguished from "vectoral" or "pumped" protons that are translocated across the membrane, although the former term is a misnomer in view of the fact that these protons are proposed to originate from the bacterial cytoplasm or the mitochondrial matrix. Through analysis of the effect of membrane potential on

the P/F and F/O equilibria (104) and time-resolved charge-translocation measurements on reconstituted enzyme (99), it has been proposed that only the $P \rightarrow F$ and $F \rightarrow O$ transitions are associated with proton translocation, each to an extent of $2H^+/e^-$. In agreement with this proposal and with the results of proton uptake measurements where two protons were determined to be bound by the enzyme upon two-electron reduction of the binuclear center (15, 59), Rich (80) suggested a model in which electron accumulation at the binuclear center drives the uptake of protons (to maintain local electroneutrality) from the i-side. These protons are stored in a proton trap close to the binuclear site but physically separated from the oxygen chemistry—in agreement with the earlier proposed histidine-cycle model by Wikström and co-workers (105; see below). Upon formation of the reactive oxygen species (i.e. the P- and F-species), protons required for water formation are taken up from the i-side and, through electrostatic repulsion, the trapped protons are expelled into the periplasm. Critical to such a scheme is the nature of the gating process that inhibits the access of the trapped protons to the i-side (i.e. prevents the trapped protons from being expelled back into the cytoplasm) and, at the same time, allows the substrate protons to enter from the i-side. Previous proposals of such a gating mechanism involve protonation and ligand exchanges on heme a_3 (83), between heme a_3 and Cu_B (113), and on Cu_B (the "histidine cycle"; 105). The latter, involving a histidine residue cycling through different conformations and protonation states, was also adapted by Iwata et al (45) on the grounds of possible multiple orientations for the Cu_B ligand His-325, because there was no electron density for the sidechain of this residue in the oxidized, azide-treated enzyme. Consistent with the Rich model, the model by Iwata et al includes two different proton access routes and accounts for strict electroneutrality.

However, recent X-ray crystallographic experiments have shown that His-325 is a Cu_B ligand in both the azide-free oxidized and the fully reduced enzymes (Harrenga et al, unpublished). The latter fact is difficult to interprete within the framework of the histidine shuttle mechanism by Iwata et al (45).

Proton-Binding Groups and Possible Proton Pumping Pathways

Upon reduction of cytochrome *c* oxidase, 2.4 H^+ have been determined to be taken up at pH 7.5 (15, 59), 0.4 of which appear to be associated with Cu_A/heme *a*, and the remaining two with the binuclear center (59). Capitanio et al (15) identified four protolytic groups undergoing reversible pK changes upon reduction of the enzyme, two of which were assigned to reduction of heme a_3 ($pK_{ox} \approx 7$, $pK_{red} > 12$, respectively), while the other two were associated with Cu_B ($pK_{ox} \approx 6$, $pK_{red} \approx 7$) and heme *a* ($pK_{ox} \approx 6$, $pK_{red} \approx 9$), respectively. In the

study by Mitchell & Rich (59) individual pKs were not accessible, indicating values <7.2 and >8.5 for the oxidized and the reduced enzyme, respectively. Somewhat differently, Ädelroth et al (1) and Hallen et al (28), studying the heme a_3–heme a backward electron transfer (after flashing off CO from the mixed-valence enzyme) by following conductance and/or absorbance changes, identified a protonatable group close to the binuclear site to which they assigned pKs of 9.7 and 8.5 for reduced and oxidized heme a_3, respectively. Hallen et al (28) have speculated that a hydroxide ion bound to the binuclear center could be the proton-binding group. Such a hydroxide ion has been suggested as a ligand to Cu_B on the grounds of EXAFS and ENDOR measurements on an oxidized aa_3 type quinol oxidase enzyme at high pH (22). Additionally, it could provide the group close to the binuclear center suggested by Verkhovsky et al (95), the protonation of which is required to stabilize the reduced form of heme a_3.

Two possible proton pathways were identified in the *Paracoccus denitrificans* enzyme (45), here referred to as the D- and K-pathways, respectively (see above). The former involves, besides a number of polar residues, the highly conserved Asp-124 and Glu-278, while the latter leads toward the binuclear center via Lys-354. Mutation of Asp-124 to asparagine produces an enzyme that, though still able to reduce oxygen (albeit with a lower activity), is incapable of proton pumping (88), an effect that can be reversed by second-site mutations in the close vicinity of the aspartate (24). Thus, Iwata et al (45) assigned the D-pathway to the translocated protons and the K-pathway to the substrate protons. Such an assignment is also compatible with the observation that terminal oxidases that are expected not to pump protons, e.g. those from archaea, do not possess acidic residues homologous to Asp-124 and Glu-278, while Lys-354 is conserved in these enzymes.

From additional site-directed mutagenesis experiments (43, 44, 50a, 85, 87, 100), it has now become clear that Asp-124, Glu-278, and Lys-354 are indeed key residues for proton transfer to the binuclear site. However, the fact that heme a_3 reduction is inhibited by mutation of Lys-354 to Met (44) and the results of charge-translocation studies (50a, 85) suggest that the lysine is required for the $O \rightarrow R$ transition but it does not seem to be crucial for the $P \rightarrow O$ part of the catalytic cycle. Additionally, mutation of Glu-278 was found to completely inhibit proton translocation associated with the $P \rightarrow O$ reactions (50a, 85), therefore suggesting the two channels to be important for different parts of the catalytic cycle rather than for consumed and pumped protons. One could speculate that oxygen binding to the binuclear center blocks proton access via the K-pathway, e.g. through interaction of the oxygen with Tyr-280 or through structural changes coupled to the reduction of the binuclear site that could block

the K-path and/or open the D-path. Such changes could be triggered by Cu_B and heme a_3 moving apart upon reduction as the proposed hydroxide group bound between the two redox sites becomes protonated.

CONCLUSIONS

Substantial progress toward understanding the mechanism of cytochrome *c* oxidase action has been made in recent years. First, mainly by time-resolved optical and resonance Raman spectroscopy, the catalytic cycle has been investigated and the intermediates have been identified and characterized, although there is some debate about the structure of one major intermediate. Second, site-directed mutagenesis work has provided a good structural picture of the enzyme, e.g. it has led to the identification, in combination with spectroscopy, of the ligands to the metals. Site-directed mutagenesis work has also identified some residues that are involved in proton transfer. Third, two independent structure determinations, one of a bacterial and the other of a mitochondrial cytochrome *c* oxidase, have yielded a detailed view into the molecular architecture of cytochrome *c* oxidase. The arrangement of the prosthetic groups and the structures of the protein subunits are now precisely known. Putative proton transfer pathways have been identified, supported by the results of site-directed mutagenesis experiments. The characterization of such mutants has led to a better understanding of the roles of the proton transfer pathways.

However, neither the structural nor the spectroscopic work has led to a convincing proposal how the redox chemistry of oxygen reduction and water formation is coupled to proton pumping. Two basic mechanisms are discussed: direct coupling versus indirect coupling. Indirect coupling would be caused by a structural change distant from the active site that leads to proton release to the outside, whereas in a direct coupling mechanism a change of a ligand to a metal of the binuclear site would be critically involved in proton pumping. Very attractive is the hypothesis (80, 105) that the protons, which are taken up upon reduction of the enzyme, are those being pumped. They would, through electrostatic interactions, be "expelled" by protons, which are taken up later and are "consumed" in the catalytic cycle.

It can be hoped that it will be possible to trap intermediates of the catalytic cycle in the crystals and to determine their structures. These structures should form the cornerstone for a further elucidation of the mechanism, but further spectroscopic experiments will be needed. It will be of critical importance to identify those residues or groups that are protonated upon reduction. Fourier transform infrared spectroscopy using wild-type and mutant enzymes both under steady state conditions (35a, 55a) and kinetic experiments should be very helpful. Thus, there are good reasons to believe that we will understand the

mechanism of the coupling of redox chemistry and proton pumping in cytochrome *c* oxidase within a few years.

Literature Cited

1. Ädelroth P, Sigurdson H, Hallen S, Brzezinski P. 1996. Kinetic coupling between electron and proton transfer in cytochrome *c* oxidase: simultaneous measurements of conductance and absorbance changes. *Proc. Natl. Acad. Sci. USA* 93:12292–97
2. Adman ET. 1991. Copper protein structures. *Adv. Protein Chem.* 42:145–97
3. Alben JO, Moh PP, Fiamingo FG, Altschuld RA. 1981. Cytochrome oxidase (a_3) heme and copper observed by low temperature Fourier-transform infrared spectroscopy of the CO complex. *Proc. Natl. Acad. Sci. USA* 78:234–37
4. Antalis TM, Palmer G. 1982. Kinetic characterization of interaction between cytochrome oxidase and cytochrome *c*. *J. Biol. Chem.* 257:6194–206
5. Babcock GT, Varotsis C. 1993. Discrete steps in dioxygen activation—the cytochrome oxidase/O_2 reaction. *J. Bioenerg. Biomembr.* 25:71–80
6. Babcock GT, Wikström M. 1992. Oxygen activation and the conservation of energy in cell respiration. *Nature* 356:301–9
7. Babcock GT, Floris R, Nilsson T, Pressler M, Varotsis C, Vollenbroek E. 1996. Dioxygen activation in enzymatic systems and in inorganic models. *Inorg. Chim. Acta* 243:345–53
8. Bailey JA, James CA, Woodruff WH. 1996. Flow-flash kinetics of O_2 binding to cytochrome *c* oxidase at elevated [O_2]: observations using high-pressure stopped-flow for gaseous reactants. *Biochem. Biophys. Res. Commun.* 220:1055–60
9. Bickar D, Bonaventura J, Bonaventura C. 1982. Cytochrome *c* oxidase binding of hydrogen peroxide. *Biochemistry* 21: 2661–66
10. Blackburn NJ, Barr ME, Woodruff WH, van der Oost J, DeVries S. 1994. Metal-metal bonding in biology—EXAFS evidence for a 2.5 Å copper-copper bond in the Cu_A center of cytochrome *c* oxidase. *Biochemistry* 33:10401–7
11. Blackmore RS, Greenwood C, Gibson QH. 1991. Studies of the primary oxygen intermediate in the reaction of fully reduced cytochrome oxidase. *J. Biol. Chem.* 266:19245–49
12. Blair DF, Witt SN, Chan SI. 1985. Mechanism of cytochrome *c* oxidase-catalyzed dioxygen reduction at low temperatures: evidence for two intermediates at the three-electron level and entropic promotion of the bond-breaking step. *J. Am. Chem. Soc.* 107:7389–99
13. Brzezinski P. 1996. Internal electron-transfer reactions in cytochrome *c* oxidase. *Biochemistry* 35:5611–15
14. Capitanio N, Capitanio G, Demarinis DA, De Nitto E, Massari S, Papa S. 1996. Factors affecting the H^+/e^- stoichiometry in mitochondrial cytochrome *c* oxidase: influence of the rate of electron flow and transmembrane pH. *Biochemistry* 35:10800–6
15. Capitanio N, Vygodina TV, Capitanio C, Konstantinov AA, Nicholls P, Papa S. 1997. Redox-linked protolytic reactions in soluble cytochrome *c* oxidase from beef-heart mitochondria: redox Bohr effects. *Biochim. Biophys. Acta* 1318:255–65
16. Calhoun MW, Thomas JW, Gennis RG. 1994. The cytochrome oxidase superfamily of redox-driven proton pumps. *Trends Biochem. Sci.* 19:325–30
17. Castresana J, Lübben M, Saraste M, Higgins DG. 1994. Evolution of cytochrome oxidase, an enzyme older than atmospheric oxygen. *EMBO J.* 13:2516–25
18. Chance B, Saronio C, Leigh JS Jr. 1975. Functional intermediates in the reaction of membrane-bound cytochrome oxidase with oxygen. *J. Biol. Chem.* 250:9226–37
19. Clore GM, Andréasson L-E, Karlsson BG, Aasa R, Malmström B. 1980. Characterization of the low-temperature intermediates of the reaction of fully reduced soluble cytochrome oxidase with oxygen by electron paramagnetic resonance and optical spectroscopy. *Biochem. J.* 185:139–54
20. Dyer RB, Einarsdottir O, Killough PM,

Lopez-Garcia JJ, Woodruff WH. 1989. Transient binding of photodissociated CO to Cu_B^+ of eucaryotic cytochrome oxidase at ambient temperature. *J. Am. Chem. Soc.* 111:7657–59
21. Fabian M, Palmer G. 1995. The interaction of cytochrome oxidase with hydrogen peroxide: the relationship of compounds P and F. *Biochemistry* 34:13802–10
22. Fann YC, Ahmed I, Blackburn NJ, Boswell JS, Verkhovskaya ML, et al. 1995. Structure of Cu_B in the binuclear heme-copper center of the cytochrome aa_3-type quinol oxidase from *Bacillus subtilis. Biochemistry* 35:10245–55
23. Ferguson-Miller S, Babcock GT. 1996. Heme/copper terminal oxidases. *Chem. Rev.* 96:2889–907
24. Garcia-Horsman JA, Puustinen A, Gennis RB, Wikström M. 1995. Proton transfer in cytochrome bo_3 ubiquinol oxidase of *Escherichia coli*: second-site mutations in subunit I that restore proton pumping in the mutant Asp–135 Asn. *Biochemistry* 34:4428–33
25. Gibson QH, Greenwood C. 1963. Reactions of cytochrome oxidase with oxygen and carbon monoxide. *Biochem. J.* 86:541–54
26. Green GN, Fang H, Lin RJ, Hewton G, Mather M, et al. 1988. The nucleotide sequence of the cyd locus encoding the two subunits of the cytochrome *d* terminal oxidase complex of *Escherichia coli*. *J. Biol. Chem.* 263:13138–43
27. Greenwood C, Gibson QH. 1967. The reaction of reduced cytochrome *c* oxidase with oxygen. *J. Biol. Chem.* 242:1782–87
28. Hallen S, Brzezinski P, Malmström BG. 1994. Internal electron transfer in cytochrome *c* oxidase is coupled to the protonation of a group close to the bimetallic site. *Biochemistry* 33:1467–72
29. Hallen S, Nilsson T. 1992. Proton transfer during the reaction of fully reduced cytochrome *c* oxidase and dioxygen: pH and deuterium isotope effects. *Biochemistry* 31:11853–59
30. Haltia T, Finel M, Harms N, Nakari T, Raitio M, et al. 1989. Deletion of the gene for subunit III leads to defective assembly of bacterial cytochrome oxidase. *EMBO J.* 8:3571–79
31. Han S, Ching Y, Rousseau DL. 1989. Evidence for a hydroxide intermediate in cytochrome *c* oxidase. *J. Biol. Chem.* 264:6604–7
32. Han S, Ching Y, Rousseau DL. 1990. Primary intermediate in the reaction of oxygen with fully reduced cytochrome *c* oxidase. *Proc. Natl. Acad. Sci. USA* 87:2491–95
33. Han S, Ching Y, Rousseau DL. 1990. Ferryl and hydroxy intermediates in the reaction of oxygen with reduced cytochrome *c* oxidase. *Nature* 348:89–90
34. Han S, Ching Y, Rousseau DL. 1990. Cytochrome *c* oxidase: decay of the primary oxygen intermediate involves direct electron transfer from cytochrome *a*. *Proc. Natl. Acad. Sci. USA* 87:8408–12
35. Hansson O, Karlsson B, Aasa R, Vänngård T, Malmström BG. 1982. The structure of the paramagnetic oxygen intermediate in the cytochrome *c* oxidase reaction. *EMBO J.* 1:1295–97

35a. Hellwig P, Rost P, Kaiser U, Ostermeier C, Michel H, Mäntele W. 1996. Carboxyl group protonation upon reduction of the *Paracoccus denitrificans* cytochrome *c* oxidase: direct evidence by FTIR spectroscopy. *FEBS Lett.* 385:53–57

36. Hendler RW, Pardhasaradhi K, Reynafarje B, Ludwig B. 1991. Comparison of energy-transducing capabilities of the two- and three-subunit cytochromes aa_3 from *Paracoccus denitrificans* and the 13-subunit beef heart enzyme. *Biophys. J.* 60:415–23
37. Hill BC. 1991. The reaction of the electrostatic cytochrome *c*–cytochrome oxidase complex with oxygen. *J. Biol. Chem.* 266:2219–26
38. Hill BC. 1994. Modelling the sequence of electron transfer reactions in the single turnover of reduced, mammalian cytochrome *c* oxidase with oxygen. *J. Biol. Chem.* 269:2419–25
39. Hill BC, Greenwood C. 1983. Spectroscopic evidence for the participation of compound A (Fe_{a3}^{2+}-O_2) in the reaction of mixed-valence cytochrome *c* oxidase with oxygen at room temperature. *Biochem. J.* 215:659–67
40. Hill BC, Greenwood C. 1984. The reaction of fully reduced cytochrome *c* oxidase with oxygen studied by flow-flash spectrophotometry at room temperature. *Biochem. J.* 218:913–21
41. Hill BC, Marmor S. 1991. Photochemical and ligand-exchange properties of the cyanide complex of fully reduced cytochrome *c* oxidase. *Biochem. J.* 279: 355–60
42. Hirota S, Mogi T, Ogura T, Hirano T, Anraku Y, et al. 1994. Observation of the Fe-O_2 and Fe^{IV}=O stretching Raman bands for dioxygen reduction intermediates of cytochrome *bo* isolated from *Escherichia coli*. *FEBS Lett.* 352:67–70
43. Hosler JP, Ferguson-Miller S, Calhoun

MW, Thomas JW, Hill J, et al. 1993. Insight into the active-site structure and function of cytochrome oxidase by analysis of site-directed mutants of bacterial cytochrome aa_3 and cytochrome *bo*. *J. Bioenerg. Biomembr.* 25:121–36

44. Hosler JP, Shapleigh JP, Mitchell DM, Kim Y, Pressler MA, et al. 1996. Polar residues in helix VIII of subunit I of cytochrome *c* oxidase influence the activity and the structure of the active site. *Biochemistry* 35:10776–83
45. Iwata S, Ostermeier C, Ludwig B, Michel H. 1995. Structure at 2.8 Å resolution of cytochrome *c* oxidase from *Paracoccus denitrificans*. *Nature* 376:660–69
46. Kadenbach B. 1986. Regulation of respiration and ATP synthesis in higher organisms: hypothesis. *J. Bioenerg. Biomembr.* 18:39–54
47. Karlsson B, Aasa R, Vänngård T, Malmström BG. 1981. An EPR-detectable intermediate in the cytochrome oxidase-dioxygen reaction. *FEBS Lett.* 131:186–88
48. Kelly M, Lappalainen P, Talbo G, Haltia T, van der Oost J, Saraste M. 1993. Two cysteines, two histidines, and one methionine are ligands of a binuclear purple copper center. *J. Biol. Chem.* 268:16781–87
49. Kitagawa T, Ogura T. 1997. Oxygen activation mechanism at the binuclear site of heme-copper oxidase superfamily as revealed by time-resolved resonance Raman spectroscopy. *Progr. Inorg. Chem.* 45:431–479
50. Konstantinov AA, Capitanio N, Vygodina TV, Papa S. 1992. pH changes associated with cytochrome *c* oxidase reaction with H_2O_2: protonation state of the peroxy and oxoferryl intermediates. *FEBS Lett.* 312:71–74

50a. Konstantinov AA, Siletsky S, Mitchell D, Kaulen A, Gennis RB. 1997. The roles of the two proton input channels in cytochrome *c* oxidase from *Rhodobacter sphaeroides* probed by the effects of site-directed mutations on time-resolved electrogenic intraprotein proton transfer. *Proc. Natl. Acad. Sci. USA* 94:9085–90

51. Kraulis PJ. 1991. MOLSCRIPT: a program to produce both detailed and schematic plots of protein structure. *J. Appl. Crystallogr.* 24:946–50
52. Kuhn-Neutwig L, Kadenbach B. 1985. Isolation and properties of cytochrome *c* oxidase from rat liver and quantification of immunological differences between isoforms from various rat tissues with subunit-specific antisera. *Eur. J. Biochem.* 149:147–58
53. Lappalainen P, Watmough NJ, Greenwood C, Saraste M. 1995. Electron transfer between cytochrome *c* and the isolated Cu_A domain: identification of substrate-binding residues in cytochrome *c* oxidase. *Biochemistry* 34:5824–30
54. Larsson S, Källebring B, Wittung P, Malmström BG. 1995. The Cu_A center of cytochrome-c oxidase: electronic structure and spectra of models compared to the properties of Cu_A domains. *Proc. Natl. Acad. Sci. USA* 92:7167–71
55. Lauraeus M, Morgan JE, Wikström M. 1993. Peroxy and ferryl intermediates of the quinol-oxidizing cytochrome aa_3 from *Bacillus subtilis*. *Biochemistry* 32:2664–70

55a. Lübben M, Gerwert K. 1996. Redox FTIR difference spectroscopy using caged electrons reveals contributions of carboxyl groups to the catalytic mechanism of haem-copper oxidases. *FEBS Lett.* 397:303–7

56. Ludwig B, Gibson QH. 1981. Reaction of oxygen with cytochrome *c* oxidase from *Paracoccus denitrificans*. *J. Biol. Chem.* 256:10092–98
57. Malatesta F, Antonini G, Sarti P, Brunori M. 1995. Structure and function of a molecular machine–cytochrome *c* oxidase. *Biophys. Chem.* 54:1–33
58. Merrit EA, Murphy MEP. 1994. Raster 3D version 2.0: a program for photorealistic molecular graphics. *Acta Crystallogr.* 50:869–73
59. Mitchell R, Rich PR. 1994. Proton uptake by cytochrome *c* oxidase on reduction and on ligand binding. *Biochim. Biophys. Acta* 1186:19–26
60. Morgan JE, Verkhovsky MI, Puustinen A, Wikström M. 1995. Identification of a "peroxy" intermediate in cytochrome bo_3 of *Escherichia coli*. *Biochemistry* 34:15633–37
61. Morgan JE, Verkhovsky MI, Wikström M. 1996. Observation and assignment of peroxy and ferryl intermediates in the reduction of dioxygen to water by cytochrome *c* oxidase. *Biochemistry* 35:12235–40
62. Moody AJ, Brandt U, Rich PR. 1991. Single electron reduction of "slow" and "fast" cytochrome *c* oxidase. *FEBS Lett.* 293:101–5
63. Oertling WA, Kean RT, Wever R, Babcock GT. 1990. Factors affecting the iron-oxygen vibrations of ferrous oxy and ferryl oxo heme proteins and model compounds. *Inorg. Chem.* 29:2633–45

64. Ogura T, Takahashi S, Shinzawa-Itoh K, Yoshikawa S, Kitagawa T. 1990. Observation of the Fe^{4+}=O stretching Raman band for cytochrome oxidase compound B at ambient temperature. *J. Biol. Chem.* 265:14721–23
65. Ogura T, Takahashi S, Shinzawa-Itoh K, Yoshikawa S, Kitagawa T. 1991. Time-resolved resonance Raman investigation of cytochrome oxidase catalysis: observation of a new oxygen-isotope sensitive Raman band. *Bull. Chem. Soc. Jpn.* 64: 2901–7
66. Ogura T, Takahashi S, Hirota S, Shinzawa-Itoh K, Yoshikawa S, et al. 1993. Time-resolved resonance Raman elucidation of the pathway for dioxygen reduction by cytochrome *c* oxidase. *J. Am. Chem. Soc.* 115:8527–36
67. Ogura T, Hirota S, Proshlyakov DA, Shinzawa-Itoh K, Yoshikawa S, Kitagawa T. 1996. Time-resolved resonance Raman evidence for tight coupling between electron transfer and proton pumping of cytochrome *c* oxidase upon the change from the Fe(V) oxidation level to the Fe(IV) oxidation level. *J. Am. Chem. Soc.* 118:5443–49
68. Oliveberg M, Brzezinski P, Malmström BG. 1989. The effect of pH and temperature on the reaction of fully reduced and mixed-valence cytochrome *c* oxidase with dioxygen. *Biochim. Biophys. Acta* 977:322–28
69. Oliveberg M, Malmström BG. 1992. Reaction of dioxygen with cytochrome *c* oxidase reduced to different degrees: indications of a transient dioxygen complex with copper-B. *Biochemistry* 31:3560–63
70. Orii Y. 1988. Intermediates in the reaction of reduced cytochrome oxidase with dioxygen. *Ann. NY Acad. Sci.* 550:105–17
71. Ostermeier C, Iwata I, Ludwig B, Michel H. 1995. F_v fragment–mediated crystallization of the membrane protein bacterial cytochrome *c* oxidase. *Nat. Struct. Biol.* 2:842–46
72. Ostermeier C, Harrenga A, Ermler U, Michel H. 1997. Structure at 2.7 Å resolution of the *Paracoccus denitrificans* two-subunit cytochrome *c* oxidase complexed with an antibody F_v-fragment. *Proc. Natl. Acad. Sci. USA* 94:10547–53
73. Palmer G, Babcock GT, Vickery LE. 1976. A model for cytochrome oxidase. *Proc. Natl. Acad. Sci. USA* 73:2206–10
74. Preisig O, Anthamatten D, Hennecke H. 1993. Genes for a microaerobically induced oxidase complex in *Bradyrhizobium japonicum* are essential for a nitrogen-fixing endosymbiosis. *Proc. Natl. Acad. Sci. USA* 90:3309–13
75. Proshlyakov DA, Ogura T, Shinzawa-Itoh K, Yoshikawa S, Appelman EH, et al. 1994. Selective resonance Raman observation of the "607 nm" form generated in the reaction of oxidized cytochrome *c* oxidase with hydrogen peroxide. *J. Biol. Chem.* 269:29385–88
76. Proshlyakov DA, Ogura T, Shinzawa-Itoh K, Yoshikawa S, Kitagawa T. 1996. Resonance Raman/absorption characterization of the oxo intermediates of cytochrome *c* oxidase generated in its reaction with hydrogen peroxide: pH and H_2O_2 concentration dependence. *Biochemistry* 35:8580–86
77. Proshlyakov DA, Ogura T, Shinzawa-Itoh K, Yoshikawa S, Kitagawa T. 1996. Microcirculating system for simultaneous determination of Raman and absorption spectra of enzymatic reaction intermediates and its application to the reaction of cytochrome *c* oxidase with hydrogen peroxide. *Biochemistry* 35:76–82
78. Puustinen A, Verkhovsky MI, Morgan JE, Belevich NP, Wikström M. 1996. Reaction of the *Escherichia coli* quinol oxidase cytochrome bo_3 with dioxygen: the role of a bound ubiquinone molecule. *Proc. Natl. Acad. Sci. USA* 93:1545–48
79. Ramirez BE, Malmström BG, Winkler JR, Gray HB. 1995. The currents of life: the terminal electron-transfer complex of respiration. *Proc. Natl. Acad. Sci. USA* 92:11949–51
80. Rich PR. 1995. Towards an understanding of the chemistry of oxygen reduction and proton translocation in the iron-copper respiratory oxidases. *Aust. J. Plant Physiol.* 22:479–86
81. Rieder R, Bosshard HR. 1980. Comparison of the binding sites on cytochrome *c* for cytochrome *c* oxidase, cytochrome bc_1, and cytochrome c_1. Differential acetylation of lysyl residues in free and complexed cytochrome *c*. *J. Biol. Chem.* 255:4732–39
82. Riistama S, Puustinen A, Garcia-Horsman A, Iwata S, Michel H, et al. 1996. Channeling of dioxygen into the respiratory enzyme. *Biochim. Biophys. Acta* 1275:1–4
83. Rousseau DL, Ching YC, Wang J. 1993. Proton translocation in cytochrome *c* oxidase: redox linkage through proximal ligand exchange on cytochrome a_3. *J. Bioenerg. Biomembr.* 25:165–77
84. Saraste M. 1990. Structural features of

cytochrome oxidase. *Q. Rev. Biophys.* 23: 331–66
85. Siletzky, SA, Kaulen AD, Mitchell D, Gennis RB, Konstantinov AA. 1996. Resolution of two proton conduction pathways in cytochrome *c* oxidase. *Biochim. Biophys. Acta, EBEC Rep.* 9:B27
86. Sucheta A, Georgiadis KE, Einarsdottir O. 1997. Mechanism of cytochrome *c* oxidase–catalyzed reduction of dioxygen to water: evidence for peroxy and ferryl intermediates at room temperature. *Biochemistry* 36:554–65
87. Svensson-Ek M, Thomas JW, Gennis RB, Nilsson T, Brzezinski P. 1996. Kinetics of electron and proton transfer during the reaction of wild-type and helix VI mutants of cytochrome bo_3 with oxygen. *Biochemistry* 35:13673–80
88. Thomas JW, Puustinen A, Alben JO, Gennis RB, Wikström M. 1993. Substitution of asparagine for aspartate-135 in subunit I of the cytochrome *bo* ubiquinol oxidase of *Escherichia coli* eliminates proton-pumping activity. *Biochemistry:*10923–28
89. Tsukihara T, Aoyama H, Yamashita E, Tomizaki T, Yamaguchi H, et al. 1995. Structures of metal sites of oxidized bovine heart cytochrome *c* oxidase at 2.8 Å. *Science* 269:1069–74
90. Tsukihara T, Aoyama H, Yamashita E, Tomizaki T, Yamaguchi H, et al. 1996. The whole structure of the 13-subunit oxidized cytochrome *c* oxidase at 2.8 Å. *Science* 272:1136–44
91. Varotsis C, Woodruff WH, Babcock GT. 1989. Time-resolved Raman detection of ν(Fe-O) in an early intermediate in the reduction of oxygen by cytochrome oxidase. *J. Am. Chem. Soc.* 111:6439–40
92. Varotsis C, Babcock GT. 1990. Appearance of the $\nu(Fe^{IV}{=}O)$ vibration from a ferryl-oxo intermediate in the cytochrome oxidase/dioxygen reaction. *Biochemistry* 29:7357–62
93. Varotsis C, Zhang Y, Appelman EH, Babcock GT. 1993. Resolution of the reaction sequence during the reduction of O_2 by cytochrome oxidase. *Proc. Natl. Acad. Sci. USA* 90:237–41
94. Verkhovsky MI, Morgan JE, Wikström M. 1994. Oxygen binding and activation: early steps in the reaction of oxygen with cytochrome *c* oxidase. *Biochemistry* 33:3079–86
95. Verkhovsky MI, Morgan JE, Wikström M. 1995. Control of electron delivery to the oxygen reduction site of cytochrome *c* oxidase: a role for protons. *Biochemistry* 34:7483–91
96. Verkhovsky MI, Morgan JE, Puustinen A, Wikström M. 1996a. The ferrous-oxy intermediate in the reaction of dioxygen with fully reduced cytochromes aa_3 and bo_3. *Biochemistry* 35:16241–46
97. Verkhovsky MI, Morgan JE, Puustinen A, Wikström M. 1996b. Kinetic trapping of oxygen in cell respiration. *Nature* 380:268–70
98. Verkhovsky MI, Morgan JE, Verkhouskaya ML, Wikström M. 1997. Translocation of electrical charge during a single turnover of cytochrome *c* oxidase. *Biochim. Biophys. Acta* 1318:6–10
99. Verkhovsky MI, Morgan JE, Wikström M. 1996. Redox transitions between oxygen intermediates in cytochrome *c* oxidase. *Proc. Natl. Acad. Sci. USA* 93: 12235–39
100. Vygodina TY, Mitchell D, Pecoraro C, Gennis RB, Konstantinov AA. 1996. Effect of amino acid replacements in the two proton channels of *Rh. sphaeroides* cytochrome *c* oxidase on the reaction of the enzyme with H_2O_2. *Biochim. Biophys. Acta, EBEC Rep.* 9:B32
101. Watmough NJ, Cheesman MR, Greenwood C, Thomson AJ. 1994. Cytochrome *bo* from *Escherichia coli*: reaction of the oxidized enzyme with hydrogen peroxide. *Biochem. J.* 300:469–75
102. Weng L, Baker GM. 1991. Reaction of hydrogen peroxide with the rapid form of resting cytochrome oxidase. *Biochemistry* 30:5727–33
103. Wikström M. 1981. Energy-dependent reversal of the cytochrome oxidase reaction. *Proc. Natl. Acad. Sci. USA* 78:4051–54
104. Wikström M. 1989. Identification of the electron transfers in cytochrome oxidase that are coupled to proton-pumping. *Nature* 338:776–78
105. Wikström M, Bogachev A, Finel M, Morgan JE, Puustinen A, et al. 1994. Mechanism of proton translocation by the respiratory oxidases: the histidine cycle. *Biochim. Biophys. Acta* 1187:106–11
106. Wikström M, Morgan JE. 1992. The dioxygen cycle: spectral, kinetic, and thermodynamic characteristics of ferryl and peroxy intermediates observed by reversal of the cytochrome oxidase reaction. *J. Biol. Chem.* 267:10266–73
107. Wilmanns M, Lappalainen P, Kelly M, Sauer-Eriksson E, Saraste M. 1995. Crystal structure of the membrane-exposed domain from a respiratory quinol oxidase with an engineered dinuclear copper center. *Proc. Natl. Acad. Sci. USA* 92:11954–59
108. Winkler JR, Malmström BG, Gray HB.

1995. Rapid electron injection into multiside metalloproteins: intramolecular electron transfer in cytochrome oxidase. *Biophys. Chem.* 54:199–209
109. Witt H, Ludwig B. 1997. Isolation, analysis, and deletion of the gene coding for subunit IV of cytochrome *c* oxidase in *Paracoccus denitrificans*. *J. Biol. Chem.* 272:5514–17
110. Witt H, Zickermann V, Ludwig B. 1995. Site-directed mutagenesis of cytochrome *c* oxidase reveals two acidic residues involved in the binding of cytochrome *c*. *Biochim. Biophys. Acta* 1230:74–76
111. Witt SN, Blair DF, Chan SI. 1986. Chemical and spectroscopic evidence for the formation of a ferryl Fe_{a3} intermediate during turnover of cytochrome *c* oxidase. *J. Biol. Chem.* 261:8104–7
112. Witt SN, Chan SI. 1987. Evidence for a ferryl Fe_{a3} in oxygenated cytochrome *c* oxidase. *J. Biol. Chem.* 262:1446–48
113. Woodruff WH. 1993. Coordination dynamics of heme-copper oxidases. The ligand shuttle and the control and coupling of electron transfer and proton translocation. *J. Bioenerg. Biomembr.* 25:177–88
114. Woodruff WH, Einarsdottir O, Dyer RB, Bagley KA, Palmer G, et al. 1991. Nature and functional implications of the cytochrome a_3 transients after photodissociation of CO-cytochrome oxidase. *Proc. Natl. Acad. Sci. USA* 88:2588–92
115. Wrigglesworth JM. 1984. Formation and reduction of a "peroxy" intermediate of cytochrome *c* oxidase by hydrogen peroxide. *Biochem. J.* 217:715–19
116. Yanamura W, Zhang YZ, Takamiya S, Capaldi RA. 1988. Tissue-specific differences between heart and liver cytochrome *c* oxidase. *Biochemistry* 27:4909–14
117. Yonetani T. 1961. Studies on cytochrome oxidase. III: improved preparation and some properties. *J. Biol. Chem.* 236:1680–88
118. Zickermann V, Verkhovsky M, Morgan J, Wikström M, Anemüller S, et al. 1995. Perturbation of the Cu_A site in cytochrome-c oxidase of *Paracoccus denitrificans* by replacement of Met227 with isoleucine. *Eur. J. Biochem.* 234:686–93